#619

A MEASUREMENT OF THE Σ^0-Λ^0 TRANSITION MAGNETIC MOMENT

A. Beretvas, T. Devlin *, R. Whitman

Rutgers - The State University of New Jersey

R. Handler, R. March, L. Pondrom, M. Sheaff

The University of Wisconsin

O. E. Overseth

The University of Michigan

K. Heller

The University of Minnesota

* Scientific Spokesman
Telephone: (201) 932-3531
FTS Off Net: 342-5500

I. INTRODUCTION

A. Magnetic Moments of Baryons

Precise measuremnts of baryon magnetic moments can place important constraints on any comprehensive model of hadronic structure. Predictions of moments can be just as precise as predictions of masses (1,2). A naive quark model gives a good account of the existing data on magnetic moments, with the light quark and strange quark moments as free parameters. (Table I) If one compares these quark moments with "realistic" quark masses, m, through the relation

$$\mu = g q \hbar / 2mc$$

where q is the quark charge, then one finds that g=2 is approximately true (1-5). This is strong evidence that quarks behave as pointlike, Dirac particles.

At present, isotopic spin invariance, applied to the two light quarks, accounts for the ratio of neutron to proton magnetic moments to about 3% accuracy. One cannot expect similar accuracy to apply for full SU(3) invariance. In the naive model, another parameter is required. Fermilab experiment E440 provided the first precise (<1%) measurement of a hyperon moment with $\mu_\Lambda = (-0.6138 \pm 0.0047)\mu_N$ where μ_N is the proton Bohr magneton ($\mu_N = e\hbar/2m_p c$). Since, in an s-wave quark model of baryon structure, $\mu_s = \mu_\Lambda$, this established with good precision the additional parameter needed to compute hyperon magnetic moments. Measurements of other magnetic moments provide tests of

any model.

A by-product of E440 was the first measurement of μ_{Ξ^0} (Table I). It deviates by four standard deviations from predictions based on μ_Σ. Data for a more precise measurement of μ_{Ξ^0} were taken in E495 and are presently under analysis.

It now seems likely that precise measurements of the magnetic moments of all long-lived hyperons ($\tau > 10^{-1}$ sec.) can be made with the apparatus and techniques used in E440 and E495.

A related quantity, the Σ^0-Λ^0 transition magnetic moment, is just as fundamental as the static moments. A precise measurement of $\mu_{\Sigma\Lambda}$ is the subject of this proposal.

B. The Σ^0-Λ^0 Transition Magnetic Moment

The electromagnetic matrix element between any two baryons can be written

$$\langle B' \mid H_{em} \mid B \rangle$$

It is zero unless the states B and B' satisfy the selection rules for isotopic spin, $\Delta I = 0, \pm 1$; strangeness, $\Delta S = 0$; charge, $\Delta Q = 0$. If B and B' are of like parity and the spin transition is $\Delta J = 0, \pm 1$, then the leading term in a multipole expansion is the magnetic dipole term. The diagonal matrix elements give the magnetic moments of the baryons. The off-diagonal elements give amplitudes for photoproduction and radiative decay. The only

non-zero off-diagonal matrix element between members of the lightest baryon octet is $\langle \Lambda^0 | M | \Sigma^0 \rangle$, the Σ^0-Λ^0 transition matrix element.

C. Models for Magnetic Moments

Any model or invariance principle which relates the baryon octet states to one another will yield relationships among the various matrix elements, and, thus, among the various static moments and the transition moment. The simplest model, exact SU(6) invariance (6), attempts to do this, but fails just as badly with magnetic moments as it does with masses.

All models which give a reasonable account of the existing data have an underlying broken SU(6) symmetry. The simplest of these is a naive, s-wave quark model which is described briefly here. The baryons are regarded as symmetric s-wave states of three quarks. the wave function for a spin-up u-type quark is written as $u\uparrow$, with the other five states written similarly. Some examples of the wave functions for the baryons are written below, with permutations omitted, and normalization adjusted accordingly.

$$|P\uparrow\rangle = \sqrt{\tfrac{2}{3}}\, u\uparrow u\uparrow d\downarrow - \sqrt{\tfrac{1}{3}}\left(\frac{u\uparrow u\downarrow + u\downarrow u\uparrow}{\sqrt{2}}\right) d\uparrow$$

$$|\Sigma^0\uparrow\rangle = \sqrt{\tfrac{2}{3}}\, u\uparrow d\uparrow s\downarrow - \sqrt{\tfrac{1}{3}}\left(\frac{u\uparrow d\downarrow + u\downarrow d\uparrow}{\sqrt{2}}\right) s\uparrow$$

$$|\Lambda^0\uparrow\rangle = \left(\frac{u\uparrow d\downarrow - u\downarrow d\uparrow}{\sqrt{2}}\right) s\uparrow$$

Since no orbital angular momentum exists in this model, the magnetic moment operators for the baryons can be written as the sum of the constituent quark moments

$$\mu_B \vec{\sigma}_B = \mu_1 \vec{\sigma}_1 + \mu_2 \vec{\sigma}_2 + \mu_3 \vec{\sigma}_3$$

where the numerical subscripts refer to the position in the wave function. This leads to relations such as

$$\mu_p = \frac{4}{3}\mu_u - \frac{1}{3}\mu_d$$

$$\mu_n = \frac{4}{3}\mu_d - \frac{1}{3}\mu_u$$

$$\mu_\Lambda = \mu_s$$

$$\mu_{\Sigma\Lambda} = -\sqrt{\frac{1}{3}}\,(\mu_u - \mu_d)$$

It is appropriate to use the constraint $\mu_d = -\mu_u/2$, leaving just two parameters, μ_u and μ_s. Precise measurements of nucleon and lambda moments provide the values used in Table I.

Other models (1,2) yield very similar results. The bag model (2) offers the advantage that the magnetic moments emerge in a natural way from the wave functions derived from the mass spectrum and confinement conditions without any separate parametrization of μ_u and μ_s.

II. $\Sigma^0 <---> \Lambda^0\gamma$ AND THE PRIMAKOFF EFFECT

A. The $\Sigma^0 --> \Lambda^0\gamma$ Decay Rate

The partial width for the process $\Sigma^0 --> \Lambda^0\gamma$ can be calculated from the matrix element as

$$\Gamma = 4\mu^2 K^3 \qquad (2.1)$$

where $\mu = \mu_{\Sigma\Lambda}$ and K is the photon momentum. This can be cast in a more convenient form (with $\hbar = c = 1$) as

$$\begin{aligned}\Gamma &= 4\left(\frac{\mu}{\mu_N}\right)^2\left(\frac{e}{2M_p}\right)^2\left(\frac{M_\Sigma^2 - M_\Lambda^2}{2M_\Sigma}\right)^3 \\ &= \frac{\alpha}{8}\left(\frac{\mu}{\mu_N}\right)^2\left(\frac{M_\Sigma^2 - M_\Lambda^2}{M_p M_\Sigma}\right)^3 M_p \\ &= \left(3.417 \times 10^{-3}\ MeV\right)\left(\frac{\mu}{\mu_N}\right)^2\end{aligned} \qquad (2.2)$$

Since all other decay modes are negligible in comparison to 2.2, the Σ^0 lifetime is

$$\tau = \Gamma^{-1} = (1.926 \times 10^{-19}\ \text{sec})(\mu/\mu_N)^{-2} \qquad (2.3)$$

Neither the lifetime nor the decay width is in a range which can be measured by existing techniques. Fortunately, an alternative method exists.

B. The Primakoff Effect

The inverse process, $\Lambda^0 + \gamma \rightarrow \Sigma^0$, can be studied using the nuclear Coulomb field as a source of virtual photons very close to the mass shell. The process $\Lambda^0 + (Z) \rightarrow \Sigma^0 + (Z)$ (Fig. 1) was proposed independently by Dreitlein and Primakoff (7) and Pomeranchuk and Shmushkevitch (8), and is known as the Primakoff effect. The differential cross section for the process can be written

$$\frac{d\sigma}{dq^2} = 98 \left(\frac{Z}{82}\right)^2 \left(\frac{\mu}{\mu_N}\right)^2 \frac{p_\Lambda^2}{M_\Lambda^4} \left(\frac{q_L q_T}{q^2}\right)^2 [F(q)]^2 \ mb/GeV^2 \qquad (2.4)$$

where

Z = Nuclear charge

p_Λ = incident Λ^0 momentum

$q_L = (M_\Sigma^2 - M_\Lambda^2)/2p_\Lambda$ = longitudinal momentum transfer

$q_T = p_\Lambda \sin\theta$ = transverse momentum transfer

$q^2 = q_L^2 + q_T^2$

$F(q)$ = a form factor which includes effects of the charge distribution and nuclear absorption.

This cross section (Fig. 2) vanishes at $q_T = 0$ and rises to a sharp peak at $q_T = q_L$. Thereafter, it falls off much more rapidly than any strongly interacting process. The slope parameter is typically about 10^5 GeV^{-2} compared to nuclear diffaction slopes of order 350 GeV^{-2} for uranium.

The total Primakoff cross section grows approximately as $\log(p_\Lambda)$, whereas competing strong coherent Σ° production is expected to fall with p_Λ.

For various nuclear targets with a fixed thickness, in terms of nuclear interaction length, the Primakoff cross section varies as Z^2. Alternatively, for targets with fixed number of radiation lengths, the Coulomb production is nearly independent of Z, whereas competing strong processes drop for higher Z targets.

There is a remarkable feature to this process which should be emphasized. We are accustomed to the fact that, as the momentum of a particle incident on a target increases, the characteristic distance probed becomes smaller. The Primakoff effect works in exactly the opposite way. As the energy increases, the momentum transfer decreases, and the characteristic impact parameter increases. At low energies, the process samples the charge distribution of the nucleus and is sensitive to nuclear absorption. At Fermilab energies, the process takes place entirely outside the nucleus, which can be regarded as a point charge. Nuclear absorption is small. At energies above about 300 GeV, the radius of interaction becomes comparable to the first Bohr orbit in heavy nuclei, and corrections are needed for shielding effects. The optimum energy range for doing this experiment is exactly that available in the present Fermilab neutral hyperon beam.

C. Corrections to the Primakoff Cross Section

Several corrections to the basic Primakoff cross section require consideration. These are:

1. Finite charge distribution of the nucleus,
2. Shielding of the Coulomb field by atomic electrons,
3. Hadronic absorption in the nucleus.

These effects have all been discussed by Fäldt and his collaborators (9,10). These authors show that a simple analytic treatment of nuclear absorption in a black sphere model gives a fair approximation to a more careful treatment in terms of a partially absorbing sphere. We rely on it here to simplify this discussion, and because the closed-form expression for the total cross section displays explicitly the logarithmic dependence on the kinematic variables. In this approximation the treatment of the nuclear electric form factor becomes unimportant. A prescription is given for including absorption effects in the form factor, F(q) of Eq. 2.4. The cross section can be integrated to give the total cross section as

$$\sigma = 0.496 \left(\frac{Z}{82}\right)^2 \left(\frac{\mu}{\mu_N}\right)^2 \left\{(2+u^2)\ln\left(\frac{2}{u}\right) - 2.154 + 0.4234u^2\right\} mb \qquad (2.5)$$

where $u = q_\perp R$, and $R = 1.14\ A^{1/3}$ is the nuclear radius. It is important to note that, as the energy increases, the interaction takes place at larger distances from the nucleus, and the effects of nuclear absorption decrease.

Eventually, at very high energies, the radius of the interaction gets large enough to require some correction for atomic electron shielding. This effect can also be included in F(q). The combined effects are shown for uranium in Fig. 2.

For comparison, the relative Primakoff cross section (normalized to unity at the peak) is shown for p_Λ = 15 and 150 GeV/c. At the lower momentum, characteristic of the CERN PS measurement (11), there is substantial overlap between the cross section and the region of nuclear absorption. The distortion of the log scale diminishes the apparent effect, but the CERN workers report a 34% correction to their final answer for this effect. No correction was required for atomic electron shielding.

In contrast, the proposed Fermilab experiment will require an absorption correction of about 11%, while the shielding correction will still be less than 1%.

Although the closed form of Eq. 2.5 derived from the black sphere model of Ref. 10 is adequate for this presentation, we have obtained a full optical model computer calculation of absorption effects (12), and this will be used for the final data analysis. The model is estimated to be accurate to about 5%. Since the absorption effects on our result should be of order 10%, any uncertainties in the model should affect our result well below the 1% level.

D. Competing Processes

The leading amplitude for coherent strong production of Σ^0 is Reggeon exchange which should fall off like p_Λ^{-1}. This should be negligible at Fermilab energies.

Incoherent Σ^0 production is a possible source of background. Most of it will involve additional particle production and will be eliminated by hardware or software event selection. The remainder will be spread over a much wider range of angles relative to the incident Λ^0, and will be cut or subtracted as part of the measured experimental background.

Some question arises about possible diffractive production of Σ^0. This might have the sharp nuclear diffraction shape and, within our resolution, be mistaken for Coulomb production. Two possible sources exist. First, $\Lambda \rightarrow \Lambda^* \rightarrow \Sigma + X$. The lightest candidate is Λ (1815) which decays to $\Sigma\pi$ with a c. m. momentum of 500 MeV. Second, from beam neutrons, we can also have $N \rightarrow N^* \rightarrow \Sigma K$. In this case, the lightest candidate is N(1780) for which the c. m. momentum is typically 270 MeV. In both cases, the sharp nuclear diffraction peak will be washed out by the decay, and the standard technique for subtracting hadronic background should suffice.

Dydak et al. (11) report no Σ^0 production above background except for Primakoff Σ^0's. At Fermilab, the Primakoff cross section should be higher, the backgrounds smaller, and the hadronic production of unaccompanied Σ^0 negligible.

III. EXPERIMENTAL METHOD

A. The Neutral Hyperon Facility

The experimental facilities required for this experiment are nearly identical to those used in a number of successful experiments in the neutral hyperon beam. A few changes to the detection apparatus are required and will be supplied by the experimenters. The only change in Fermilab-supplied equipment will be the substitution of a 4' dipole magnet for our present 2' magnet, and the addition of two Camac modules.

A schematic view of the apparatus is shown in Fig. 3. The M2 proton beam is incident from the left. (The vertical steering used in some other experiments is not needed here.) It strikes a Be target and neutral particles produced directly forward are selected by the hyperon sweeping magnet/collimator. The intensity and momentum spectrum for Λ^o's in this beam are well-known from previous work. We will add a lead plug in the collimator to soften the gamma rays in the beam. The neutral beam will pass through the Primakoff target just after the hyperon magnet. This will be followed by a 4' dipole to sweep out electron-positron pairs created in the target, a veto counter and a decay volume. Next is a hadron pair spectometer to detect the Λ^o decay products. Finally, at the end of the system is a lead-glass hodoscope. The upstream part of the pair spectrometer will be augmented by drift chambers for the improved angular resolution needed in this experiment.

The process of interest consists of the following sequence of events:

A Λ^0 is produced in the Be production target and survives without decay to the Primakoff target.

The Λ^0 interacts with the Coulomb field of a nucleus in the Primakoff target to produce a Σ^0.

The Σ^0 decays immediately ($\tau \approx 10^{-19}$ sec) as $\Sigma^0 \rightarrow \Lambda^0 \gamma$.

The Λ^0 passes through the veto into the vacuum chamber where it decays into $p\pi^-$ which are detected in the pair spectrometer.

The γ passes through the veto and the spectrometer aperture and strikes the lead glass hodoscope.

The fast trigger logic will consist of the absence of a count in the veto scintillator after the Primakoff target, two charged tracks in the spectrometer, and at least 5 GeV deposited in the lead glass.

The Λ^0 can be reconstructed from the two charged tracks in a standard fashion. The position and energy of the γ can be determined from the pattern of pulse heights in the lead glass. The Λ^0 and γ can be combined to determine the mass and momentum vector of the parent Σ^0. The expected mass resolution is about 5 MeV (std. dev.). Since Primakoff production is sharply peaked near forward ($\lesssim 10^{-5}$ radians), the momentum vector of the produced Σ^0 should coincide with that of the incident Λ^0. Thus it should to originate in the Be production target. These two criteria, mass and target pointing, are the principal bases for selecting Coulomb-produced Σ^0 and rejecting background.

B. Backgrounds

The principal sources of background in the proposed experiment are not real Σ^0, but other types of events which simulate the Σ^0 trigger. Over 95% of these can be eliminated in the software topological cuts.

In order to understand the nature of the remaining background events and how they can be eliminated, the characteristics of a true Primakoff event should be reviewed. In the reactions $\Lambda_1^0 + (Z) \rightarrow \Sigma^0 + (Z)$ and $\Sigma^0 \rightarrow \Lambda_2^0 + \gamma$, the Σ^0 should point back along the Λ_1^0 trajectory. The geometry for this is defined in Fig. 4(a). The Σ^0 should point back to the production target, and the deviation from this is measured by R_Σ^2. Roughly 98% of the Primakoff events should have R_Σ^2 less than 5 mm^2. (See Fig. 4(b).) The c. m. momentum of the Σ^0 decay is 74 MeV/c. Thus, $p_{T\Lambda}$ of Λ_2^0 relative to the reconstructed Σ^0 trajectory can vary from 0 to 74 Mev/c. The distribution (in terms of $p_{T\Lambda}^2$) is shown in Fig. 4(c). There is a strong peak at $p_{T\Lambda}^2 = 5.5 \times 10^{-3}$ $(GeV/c)^2$. Another useful quantity (which is highly correlated with $p_{T\Lambda}^2$ for true Σ^0, but not for backgrounds) is the target pointing parameter, R_Λ^2, for Λ_2^0, shown in Fig. 4(d). These three characteristics, the target pointing of the Σ^0 and Λ_2^0, and the transverse momentum distribution of the Λ_2^0, are powerful tools for rejecting events which have the Σ^0 topology, but which are not from Σ^0 decay. Finally, true Σ^0 events can be identified by the sharp peak in the $\Lambda_2^0 \gamma$ invariant mass distribution (Fig. 4(e)).

Two types of events dominate the background. The first is a normal beam Λ^0 (with no interaction between production and decay) which occurs with an accidental shower in the lead glass. This geometry is shown in Fig. 5(a). If such an event is reconstructed as " Σ^0 "--> $\Lambda^0 \gamma$, it will show several characteristics: the gammas are mostly below 5 GeV, the Λ^0 will point back to the production target within our resolving power (Fig. 5(d)), the " Σ^0 " will not (Fig. 5(b)), and those few events which survive cuts will generally have the wrong " Σ^0 " mass. (See Fig. 5(e).)

The second type of event which can simulate a Σ^0 is a beam Ξ^0 which decays via the sequence $\Xi^0 \rightarrow \Lambda^0 \gamma$, $\Lambda^0 \rightarrow p \pi^-$, $\pi^0 \rightarrow \gamma\gamma$, in which one of the gammas is lost, usually because it misses our detectors. The detected γ and the Λ^0 can be reconstructed to form a " Σ^0 ". The geometry is shown in Fig. 6(a). The true Ξ^0 will emanate from the production target. the c. m. momentum for its decay is 135 MeV/c. Therefore, the Λ^0 is spread over a wider distribution in p_T^2 relative to the Σ^0, (Fig. 6(c)), or relative to the target-pointing direction (Fig. 6(d)). Further, the reconstructed " Σ^0 " will generally not point back at the production target (Fig. 6(b)). Those events wich remain will be spread over a broad band of " Σ^0 " masses (Fig. 6(e)). Finally, because the production spectrum of Ξ^0 is lower than that of Λ^0, roughly half would be eliminated by cutting events with the reconstructed Σ^0 momentum below 150 GeV/c, while 85% of the true Σ^0 would survive such a cut.

The workers at CERN (11) found the Ξ^0 events to be their dominant background. This will be substantially reduced in our experiment because our detection efficiency for both gammas in the Ξ^0 events is considerably higher than theirs. Nevertheless, we expect it to be important. The beam Λ^0's with accidental showers are expected to be roughly equal in importance with the pessimistic assumptions used for expected trigger rates (Table II). The equipment design, trigger requirements and analysis procedures are strongly oriented toward reducing these backgrounds.

C. Resolving Power in p_T

It is evident from the p_T^2 distribution of Fig. 4(c) that the experimental resolution in $p_{T\Lambda}$ must be of order 10 to 20 MeV in order to distinguish the Σ^0 signal from background. (The resolution in R_Σ^2 at the target is directly related to this and the same arguments apply to it.) The apparatus as it existed for E495 had roughly 70 MeV resolution, clearly inadequate for the proposed experiment. Three improvements are proposed for the University-provided equipment:

1. The production target will be reduced in transverse dimensions to a 1 mm diameter cylinder, 0.5 interaction lengths long.
2. Drift chambers, with expected resolving power of 0.24 mm FWHM will be added to the upstream part of the pair spectrometer as shown in Fig. 3.
3. A thin (3 L_{rad}) layer of lead glass will replace the

lead converter (2 L_{rad}) which preceeds the last MWPC. This will raise the conversion efficiency for vertex location of showers with some gain in energy resolution. Even more important, it provides a means of rejecting showers which arise from hadrons hitting the lead glass hodoscope.

These changes should give an angular resolution of 0.03 mrad and a $p_{T\Lambda}$ resolution of $3 \times 10^{-5}\ p_{\Lambda}$. Further, the Σ^0 mass resolution should be improved from about 11 MeV/c^2 to better than 6 MeV/c^2. This was studied with a Monte Carlo program which accurately reproduced distributions observed in previous experiments with quite plausible assumptions about instrumental resolution. Then "improvements" were introduced. The distributions of Fig. 4-6 were generated in this way, and studies were made of the effect of cuts on signal and background.

It is useful to compare our resolving power with that of the CERN PS experiment (11). Our proposed angular resolution is about x10 better, but our energy is x10 higher, therefore, we have approximately the same resolution in p_T. All the Primakoff angular distribution will be in the smallest bin at Fermilab (see Fig. 2), whereas a non-negligible fraction of it extended into the second and third p_T^2 bins in the CERN experiment. This gave rise to some uncertainty in the extrapolation of background from high p_T^2. This problem should be absent at Fermilab.

D. Normalization and Acceptance

The Λ^0 flux can be measured in a simple, unambiguous fashion simply by allowing a pre-scaled fraction of beam Λ^0 triggers, i.e. events without the lead-glass requirement, to be recorded along with the normal Σ^0 triggers. This can be measured with target out to establish the un-attenuated Λ^0 flux. The ratio Σ^0/beam Λ^0 automatically cancels factors of geometric acceptance for the Λ^0, leaving only the γ acceptance as a geometric correction. This is a strightforward problem which has already been dealt with in our Ξ^0 experiments. The calculated efficiency is 59%, averaged over the expected momentum spectrum of Σ^0 events.

The 5 GeV trigger requirement in the lead glass eliminates 2.4% of the sigmas, and a somewhat higher software cut might raise this to 7%. This will require a small, well-understood correction.

Finally, some gammas will convert in the Primakoff target (about 31% for a 1 L_{rad} target). It will be necessary to study this effect by running with targets of different thickness, and with a goal of 2% statistical accuracy in the Primakoff cross section.

E. Rates: Real and Background

Table II shows the incident beam rates, trigger rates and losses from various cuts to be expected for a single data tape which requires about one hour of beam time. The principal backgrounds should be spread over about 30 bins (5 MeV wide) in the $\Lambda - \gamma$ invariant mass histogram, whereas 98% of the true Σ^0's should be in six bins centered at the correct mass. Thus, the background subtraction should be about 20% with these pessimistic assumptions.

F. Statistical and Systematic Uncertainties

Thirty-eight tapes such as that described in the previous section and in Table II should be taken for each of the 1 L_{rad} targets. This should give 2500 Σ^0 events on each of these targets. Sixty-three tapes are needed to get 2500 events on the 0.5 L_{rad} target. An additional 19 tapes each will be required for carbon target and target out studies of backgrounds. This gives us enough data for 2% statistical accuracy in the cross section, and 1% in the transition moment. Normalization uncertainties will be smaller.

Uncertainties in the lead glass acceptance will probably be a source of systematic error. A pessimistic estimate of this is 2% in the cross section and 1% in the moment. This rests on the fact that the inefficiency is 41% and that, pessimistically, we may determine it with 5% accuracy.

The fraction of gamma rays produced uniformly through a target which survive to emerge from it is given by

$$(1 - e^{-k})/k$$

where k = thickness/[(9/7)L_{rad}]. For a 1 L_{rad} target, this is 0.69, and for a target thickness of 0.5 L_{rad} it is 0.83. If we obtain the statistical accuracy discussed above on each of the targets, then the absorption correction should be possible with comparable accuracy.

The final statistical and systematic errors on $\mu_{\Sigma\Lambda}$ should be between 1% and 2%.

G. Comparison With The CERN Experiment

It is useful to make a point-by-point comparison of the principal features of our experiment with that of Dydak et al. (11). There are many qualitative similarities. Both are triggered by the coincidence of two charged tracks in a proportional-chamber spectrometer with at least minimum pulse height in a lead-glass array. The present proposal, however, has quantitative advantages which are shown in detail in Tables III and IV. Principal among these are the larger cross section at Fermilab energies and the high detection efficiency of our apparatus. The result is a factor of twenty more events in about one-third the data collection time, an order of magnitude improvement in signal/background ratio,and an order of magnitude improvement in the uncertainty in the final result.

IV. FACILITIES REQUIRED

A. Fermilab Facilities

This experiment requires the use of the M2 line in the Meson lab with protons at the operating Main Ring momentum (assumed to be 400 GeV) and at intensities of 10^8 to 10^9 protons per pulse. Some calibration runs at about 10^4 ppp are essential. The spill time is assumed to be 1 second. The experiment can operate with or without either of the vertical bend systems used by E361 and E555. The standard SWIC detectors for the M2 line will be needed. We need a 4' dipole just downstream of the hyperon magnet to replace a 2' magnet presently in use there.

We request a quadrupole pair for the u-shaped tunnel for smaller spot size and improved target efficiency, if possible. However, the experiment can run without it.

Other equipment needed includes the AVIS spectrometer magnet, a PDP-11 computer with Camac interface, and miscellaneous electronics from PREP. All of this has been used in previous neutral hyperon experiments. In addition, we request two 8-channel ADC Camac modules for new lead glass. Since our data collection speed is presently limited by data-logging rates, The experiment could be improved by assigning a 6250 BPI magnetic tape drive and interface to our present computer system. If the accelerator operates with a spill time of 0.5 seconds instead of 1 second, the high density drive is essential in order to avoid doubling our time estimates.

B. University Hardware

The neutral hyperon detection apparatus, in a configuration nearly the same as E495, will be required for this experiment. All of that equipment is available.

Essential new additions are several scintillation counters, two drift chambers, each capable of two-track X-Y coordinate measurements with resolution of 250 microns FWHM, a new Be production target, and four Primakoff targets. None of the targets will be hit by beam above about 10^9 ppp.

A very desirable addition is a layer of lead-glass counters to replace the lead converter between chambers P6 and P7 (Fig. 3). This will improve our ability to distinguish hadrons from gammas in the lead-glass both at the trigger level and in the off-line analysis. This addition would be generally useful in a number of experiments.

C. Personnel

The physicists committed to this work are listed below.

University of Michigan

T. Cox
J. Dworkin
O. Overseth

University of Minnesota

K. Heller

Rutgers University

A. Beretvas
L. Deck
T. Devlin
K. B. Luk
R. Ramieka
R. Whitman

University of Wisconsin

R. Handler
R. March
L. Pondrom
M. Sheaff
C. Wilkinson

R. March has commitments to Project Dumand and to a proton lifetime experiment. O. Overseth and K. Heller are involved in a neutral hyperon proposal at Brookhaven. K. Heller, in addition, is working on a proton lifetime proposal. None of the other physicists has any experimental commitments outside the M2 hyperon program at Fermilab.

Backup technical support personnel with strong commitments to this work exist at Rutgers and Wisconsin. Additional technical support is available, when needed, at Michigan and Minnesota.

D. Beam Time

The data collection time was listed in Table IV for each of the Primakoff targets. These estimates assume about one hour per data tape, which is based on previous running experience with a 1 second spill. If we run with a spill time of 0.5 seconds, all these time estimates must be doubled. The total data collection

time is 180 hours. We estimate initial tuning, calibration and trigger studies will require about 70 hours. The total request is for 250 hours of beam time.

E. Computer Time

We expect to collect about 180 data tapes. We plan to do all the analysis at Fermilab. This sould require approximately 120 hours on the new computer system.

REFERENCES

1. A. De Rujula et al., Phys. Rev. D12, 147 (1975).

2. A. Chodos et al., Phys. Rev. D10, 2599 (1974).
   T. De Grand et al., Phys. Rev. D12, 2060 (1975).

3. L. Schachinger et al., Phys. Rev. Letters 41, 1348 (1978)

4. O. W. Greenberg, Phys. Rev. Letters 13, 598 (1969).

5. H. Lipkin, Phys. Rev. Letters 41, 1629 (1978).

6. S. Coleman and S. Glashow, Phys. Rev. Letters 6, 423 (1961).

7. J. Dreitlein and H. Primakoff, Phys. Rev. 125, 1671 (1962).

8. I. Ya. Pomeranchuk and I. M. Schmushkevitch, Nucl. Phys. 23, 452 (1961).

9. G. Fäldt, Nucl. Phys. B43, 591 (1972).

10. G. Fäldt et al., Nucl. Phys. B41, 125 (1972).

11. F. Dydak et al., Nucl. Phys. B118, 1 (1977).

12. C. Wilkin, (private communication).

FIGURE CAPTIONS

Fig. 1 The Primakoff Process. A Λ^0 converts to a Σ^0 in the Coulomb field of a nucleus.

Fig. 2 The Primakoff cross section (normalized to unity at maximum) as a function of momentum transfer is shown for 15 GeV/c and 150 GeV/c incident Λ^0 momentum. Also shown is the factor F(q) which includes the effects of nuclear absorption and shielding of the Coulomb field by orbital electrons.

Fig. 3 A diagram of the apparatus, not to scale. The M2 beam is incident from the left on a Be target. The sweeper/collimator bends out charged particles and defines the neutral beam. It is followed by the Primakoff target in which the $\Lambda^0 - \Sigma^0$ transition takes place. Electron-positron pairs from the Primakoff target are swept out by the 4' magnet which follows. A veto counter selects only events where neutral particles enter the vacuum decay volume. The spectrometer consists of proportional chambers, P1-P6, two drift chambers, D1-D2, and a superconducting dipole (AVIS) with 1 GeV/c of transverse bending power. The photon detector consists of a 3Lrad converter, G1, which can be lead or a new lead glass array; a proportional chamber, P7, for vertex location, and the existing lead glass hodoscope, G2.

Fig. 4 (a) A true Primakoff event is shown in which Λ_1^0 is produced in the production target and converts to a Σ^0 in the Primakoff target. The Σ^0 is colinear with the Λ_1^0. It decays, while still in the target, to Λ_2^0 and a gamma, each of which is detected and reconstructed. The Λ_2^0 and γ trajectories are extrapolated back to the production target. The distance, R_Σ, should differ from zero only by measurement errors. For most decays, $p_{T\Lambda}^2$ (or a similar quantity, R_Λ^2) should differ substantially from zero. Distributions of Monte Carlo events are shown for (b) R_Σ^2, (c) $p_{T\Lambda}^2$, (d) R_Λ^2, and (e) $M(\Lambda^0\gamma)$.

Fig. 5 Similar to Fig. 4 for events in which a beam Λ^0 and an accidental γ simulate the topology of a Σ^0 event.

Fig. 6 Similar to Fig. 4 for events where a beam Ξ^0 decays through the sequence $\Xi^0 \rightarrow \Lambda^0\pi^0$; $\Lambda^0 \rightarrow p\,\pi^-$; $\pi^0 \rightarrow \gamma\gamma$, and in which one gamma is undetected so that the Σ^0 topology is satisfied.

Table I. Quark Model Magnetic Moments

Moment	Predicted	Observed
$\mu(p)$	2.8313	2.7928 (a,c)
$\mu(n)$	-1.8875	-1.9130 (a,d)
$\mu(\Lambda^0)$	-0.6138	-0.6138 (a)
$\mu(\Sigma^+)$	2.7213	2.95 ± 0.31 (e)
$\mu(\Sigma^0)$	0.8338	--
$\mu(\Sigma^-)$	-1.0537	-1.48 ± 0.37 (f)
$\mu(\Xi^0)$	-1.4476	-1.20 ± 0.06 (j)
$\mu(\Xi^-)$	-0.5038	-1.85 ± 0.75 (g)
$\mu(\Omega^-)$	-1.8414	--
$\mu(\Sigma^0 \to \Lambda^0 \gamma)$	-1.6346	$\lvert\mu\rvert = 1.82\ ^{+0.25}_{-0.13}$ (h)
$\mu(u)$	1.8875 (b)	--
$\mu(d)$	-0.9438 (b)	--
$\mu(s)$	-0.6138 (b)	--

NOTES:

(a) Data used as input.

(b) Parameters

(c) E. R. Cohen and B. N. Taylor, J. Phys. Chem. Ref. Data 2, 663 (1973).

(d) V. W. Cohen et al., Phys. Rev. 104, 283 (1956).

(e) N. Doble et al., Phys. Lett. 67B, 483 (1977).

(f) B. L. Roberts et al., Phys. Rev. Lett. 32, 1265 (1974).

(g) G. McD. Bingham et al., Phys. Rev. D1, 3010 (1970). R. L. Cool et al., Phys. Rev. D10, 792 (1974).

(h) F. Dydak et al., Nucl. Phys. B118, 1 (1977).

(j) G. Bunce et al. (to be published).

TABLE II

Typical Run Characteristics For One Data Tape

Protons:	5.4×10^{10} on Be Target @ 350 or 400 GeV (1.8×10^{8}/pulse for 300 spills - approx. 1 hour)
Lambdas:	3.9×10^{6} ungated " Λ° " trigger patterns 2.3×10^{6} gated " Λ° " trigger patterns 1.6×10^{4} true gated Λ° (69% yield)
Interactions:	1.0×10^{5} Λ° interactions
Sigmas:	329 Primakoff Σ° in target 227 Σ° after gamma losses in target 134 59% geometric efficiency in glass 131 2.4% loss for 5 GeV gamma cut 111 15% loss for software topology cuts

	True Σ°	" Σ° " (From Ξ°)	" Σ° " (Beam Λ° - γ)
Remaining after topology cuts	111	542	1240
$R_{\Sigma}^2 < 5$ mm^2	109	114	574
$p_{T\Lambda}^2 < 0.008$ (GeV/c)^2	108	51	536
$R_{\Lambda}^2 > 3$ mm^2	76	41	43
$P_{\Lambda} > 150$ GeV/c	67	20	41
$M(\Lambda^{\circ}\gamma) = M(\Sigma^{\circ}) \pm 15$ MeV	66	4	12

TABLE III

Comparison Of CERN PS Experiment With This Proposal

	CERN	This Proposal
Proton Beam:		
Flux (ppp)	10^{10}	10^8 - 10^9
Momentum (GeV/c)	24	400
Production Target	4 x 4 mm^2 Be	1 mm diam. Be
Photon Absorber	12 L_{rad} Pt	12 L_{rad}
Neutral Beam:		
Momentum (GeV/c)	5 - 20	80 - 350
Production Angle (mrad)	75	0
Pair Spectrometer:		
Angular Resolution (mrad)	0.4	0.03
Multiple Coulomb Scattering (mrad)	?	0.003
Mass Resolution (lambda) (MeV)	1.5	1.0
Acceptance for lambdas (average)	15%	70%
Photon Detector:		
Number of cells	84	72
Glass type	SF5	F2
Size (mm^2)	146 x 146	100 x 100
Thickness	12.7 L_{rad}	3 L_{rad} + 12 L_{rad}
Acceptance (γ from Σ^o)	10%	69%
Sigma Reconstruction:		
Mass resolution (MeV st. dev.)	5	6
Production Angle resolution (mrad)	1.5	0.05
Acceptance	1.5%	50%

TABLE IV

Target Parameters

	CERN		This Proposal				
Target	Uranium	Nickel	Lead	Lead	Nickel	Carbon	Out
Thickness (g/cm^2)	11.4	17.8	6.37	3.18	12.6	2.35	0
L/L_{rad}	1.88	1.41	1.00	0.50	1.00	0.055	-
L/L_{abs}	0.050	0.133	0.030	0.015	0.094	0.030	-
Surviving gammas	52%	61%	69%	83%	69%	98%	-
σ_{abs} (mb)	1740	730	1640	1640	730	260	-
$\sigma_{Primakoff}$ (mb)	5.1	0.64	11.1	11.1	1.51	0.079	-
Nuclear Absorption	31%	23%	11%	11%	10%	9%	-
Primakoff Branching Fraction	1/340	1/1140	1/150	1/150	1/480	1/3300	-
Number of Primakoff Events	268	89	2500	2500	2500	100	-
Signal/Background	0.6/1 (est.)	0.5/1 (est.)	4/1	2/1	4/1	0.2/1	-
Number of Tapes	?	?	38	63	38	19	19
Running time (hours)	600 total		38(a)	63(a)	38(a)	19(a)	19(a)

(a) Time estimate assumes 1 second spill time. Double running time for 0.5 second spill.

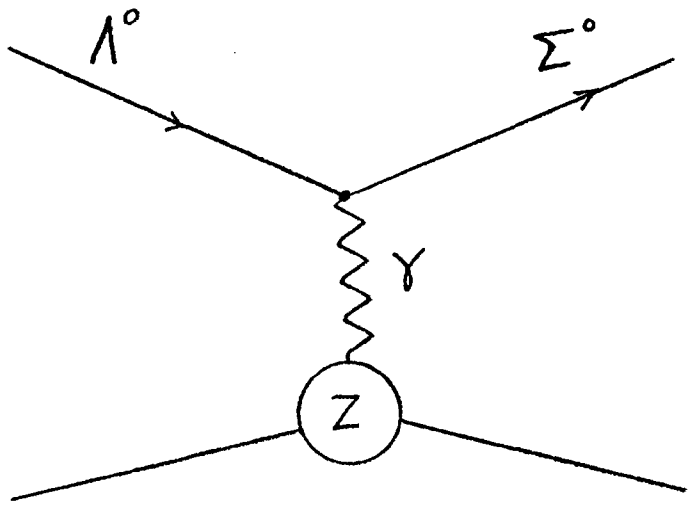

Fig. 1

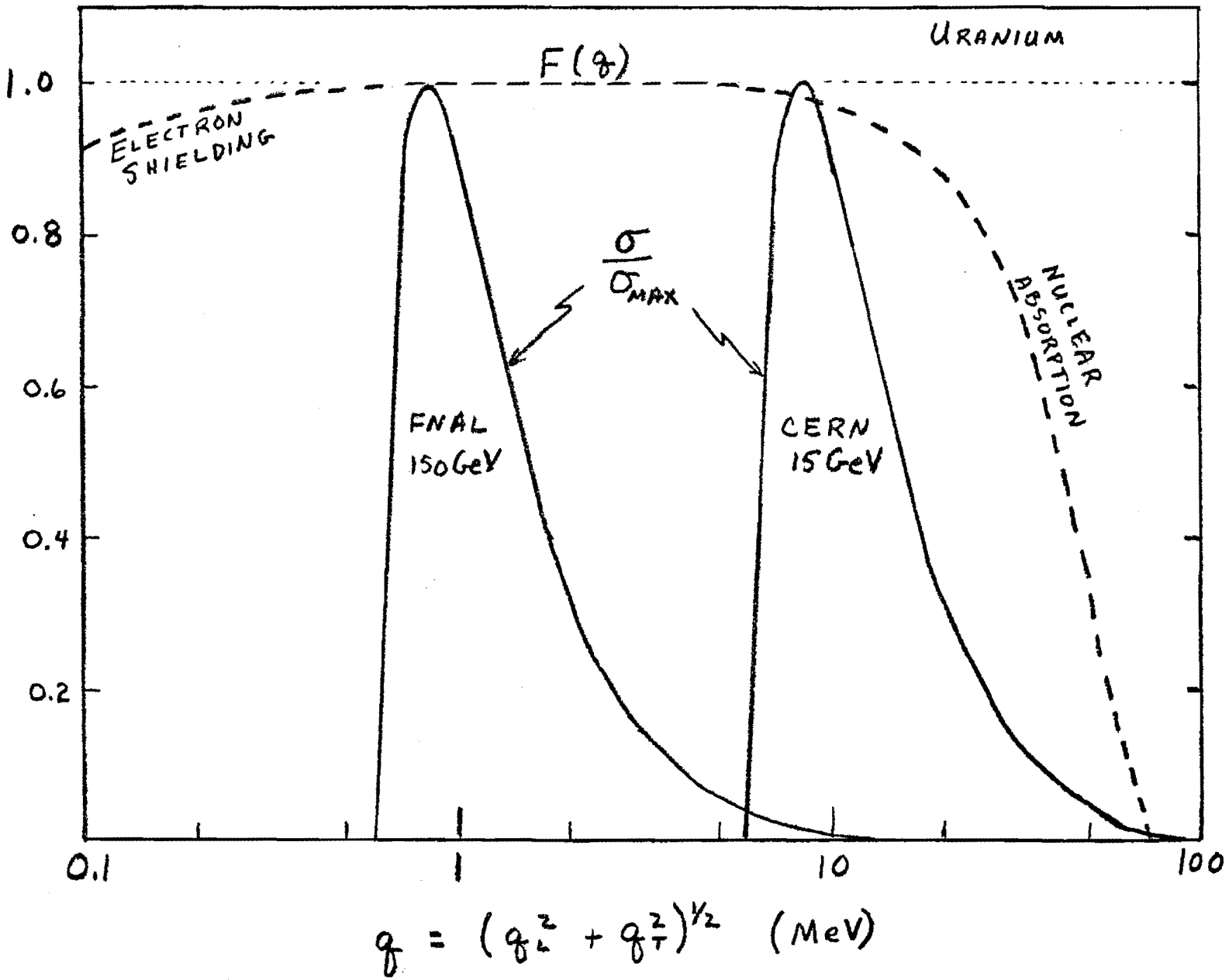
URANIUM
F(q)
1.0
0.8
0.6
0.4
0.2
ELECTRON SHIELDING
σ/σMAX
NUCLEAR ABSORPTION
FNAL 150GeV
CERN 15GeV
0.1
1
10
100
q = (qL² + qT²)^½ (MeV)

Fig. 2

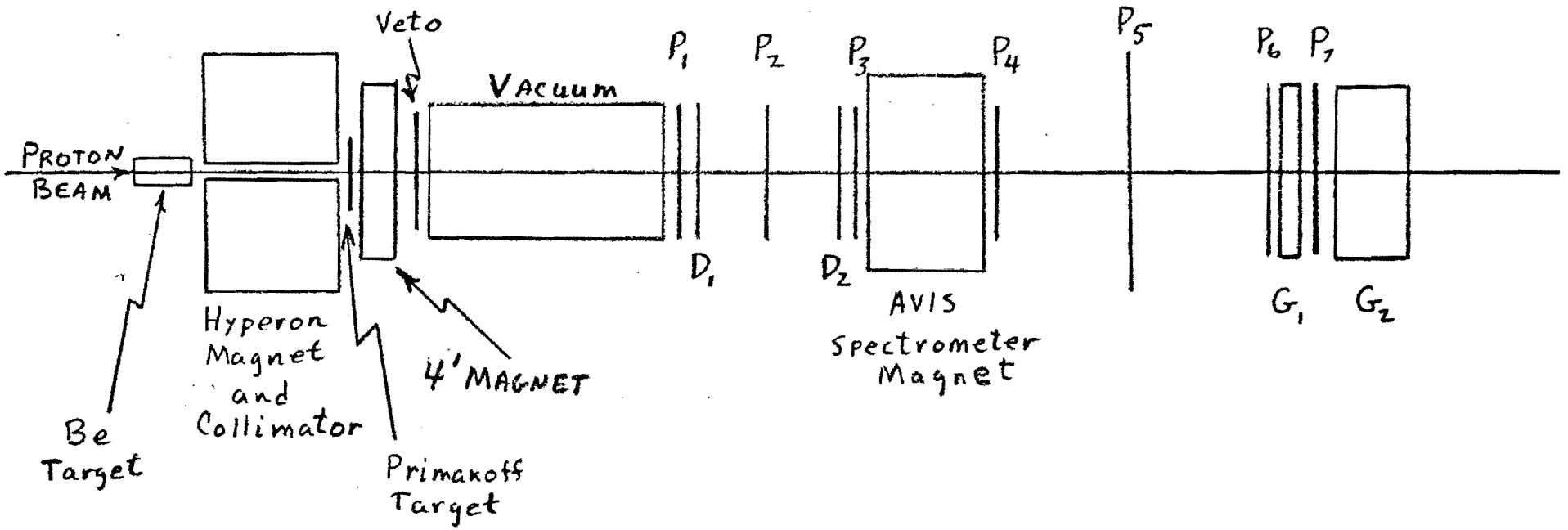
Veto
Vacuum
P_1
P_2
P_3
P_4
P_5
P_6
P_7
PROTON BEAM
D_1
D_2
AVIS Spectrometer Magnet
G_1
G_2
Hyperon Magnet and Collimator
4' MAGNET
Be Target
Primakoff Target

Fig. 3

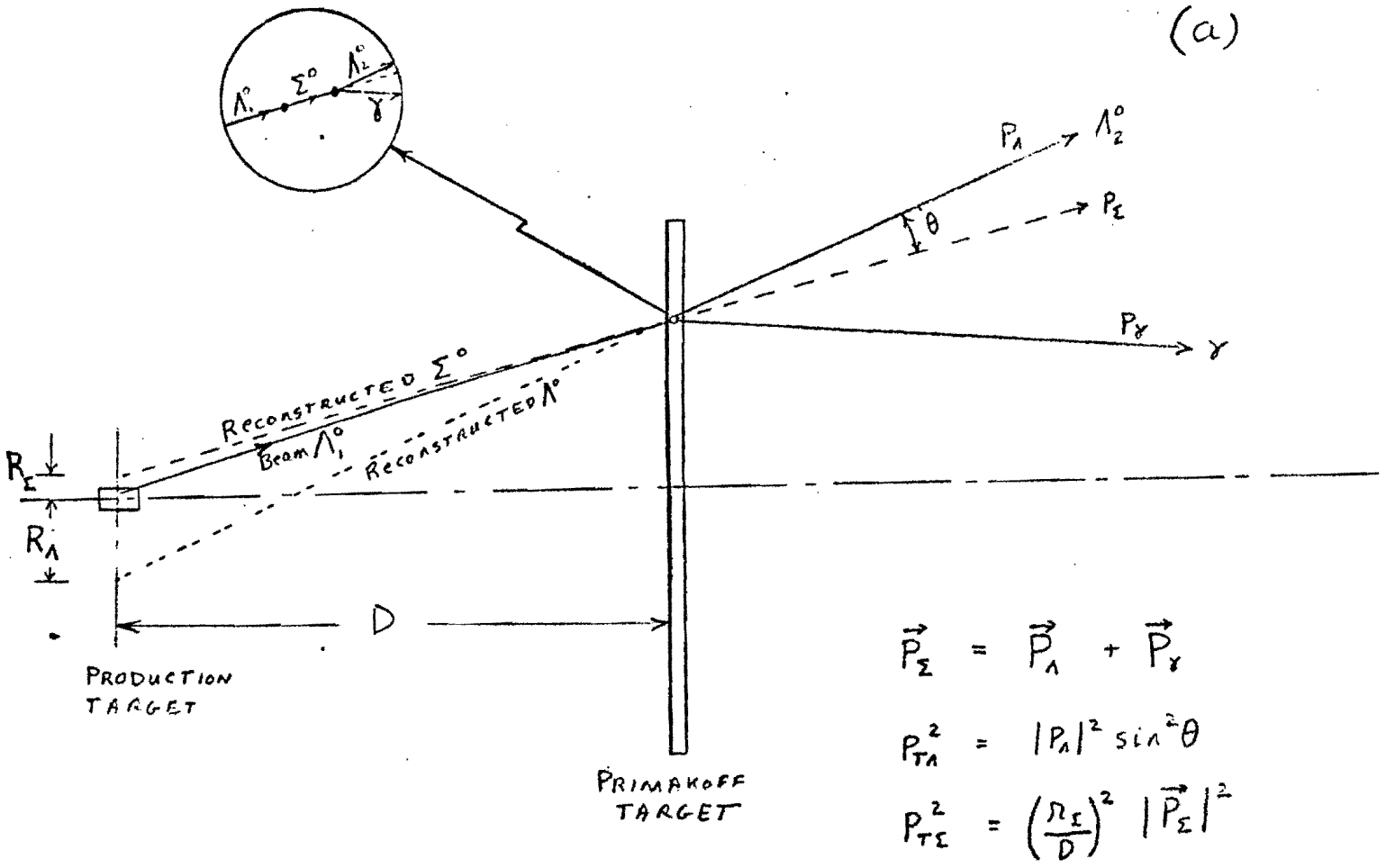
(a)
Λ^0
Σ^0
Λ_2^0
γ
P_Λ
Λ_2^0
P_Σ
θ
P_γ
γ
Reconstructed Σ^0
Beam Λ_1^0
Reconstructed Λ^0
R_Σ
R_Λ
D
PRODUCTION TARGET
PRIMAKOFF TARGET
$\vec{P}_\Sigma = \vec{P}_\Lambda + \vec{P}_\gamma$
$P_{T\Lambda}^2 = |P_\Lambda|^2 \sin^2\theta$
$P_{T\Sigma}^2 = \left(\frac{R_\Sigma}{D}\right)^2 |\vec{P}_\Sigma|^2$

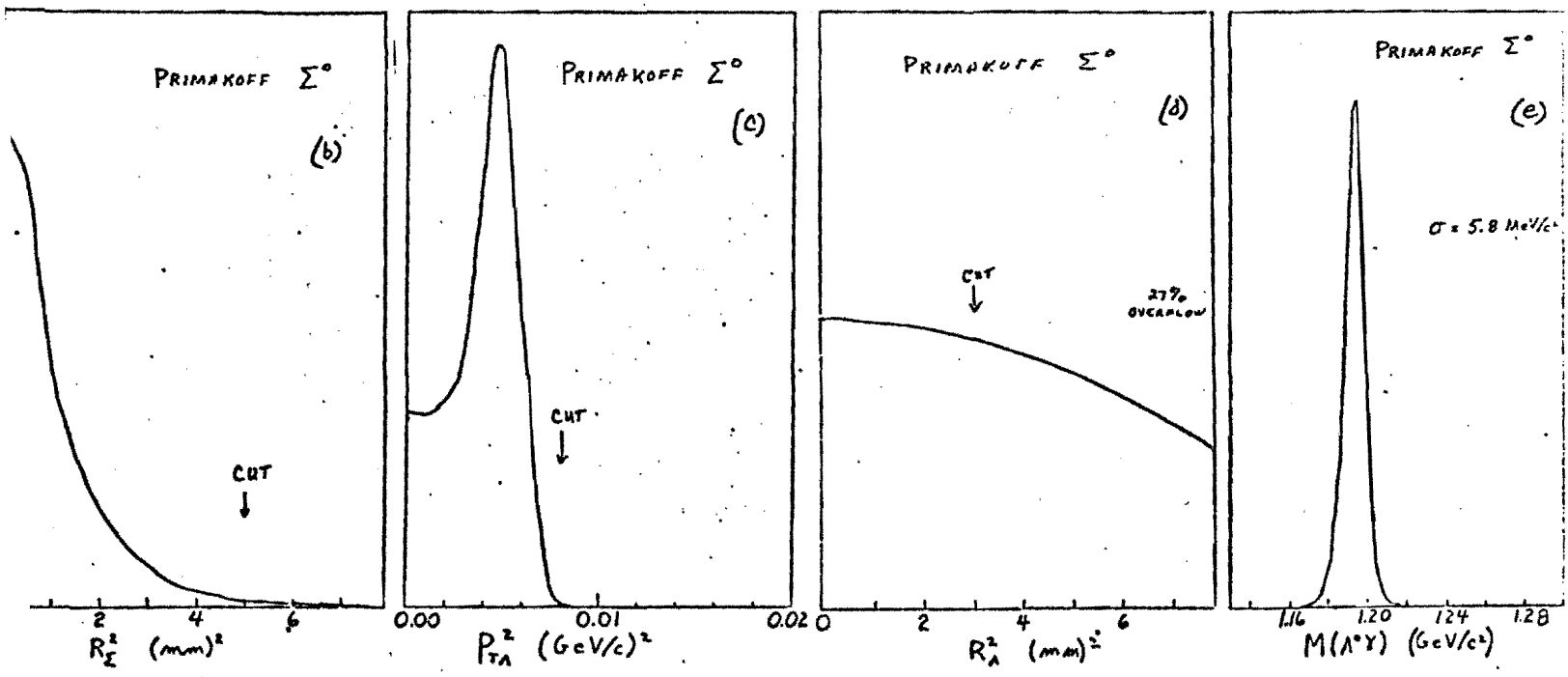
PRIMAKOFF Σ^0
(b)
CUT
2
4
6
R_Σ^2 (mm)^2
PRIMAKOFF Σ^0
(c)
CUT
0.00
0.01
0.02
$P_{T\Lambda}^2$ (GeV/c)^2
PRIMAKOFF Σ^0
(d)
CUT
27% OVERFLOW
0
2
4
6
R_Λ^2 (mm)^2
PRIMAKOFF Σ^0
(e)
σ = 5.8 MeV/c^2
1.16
1.20
1.24
1.28
M($\Lambda^0\gamma$) (GeV/c^2)

Fig. 4

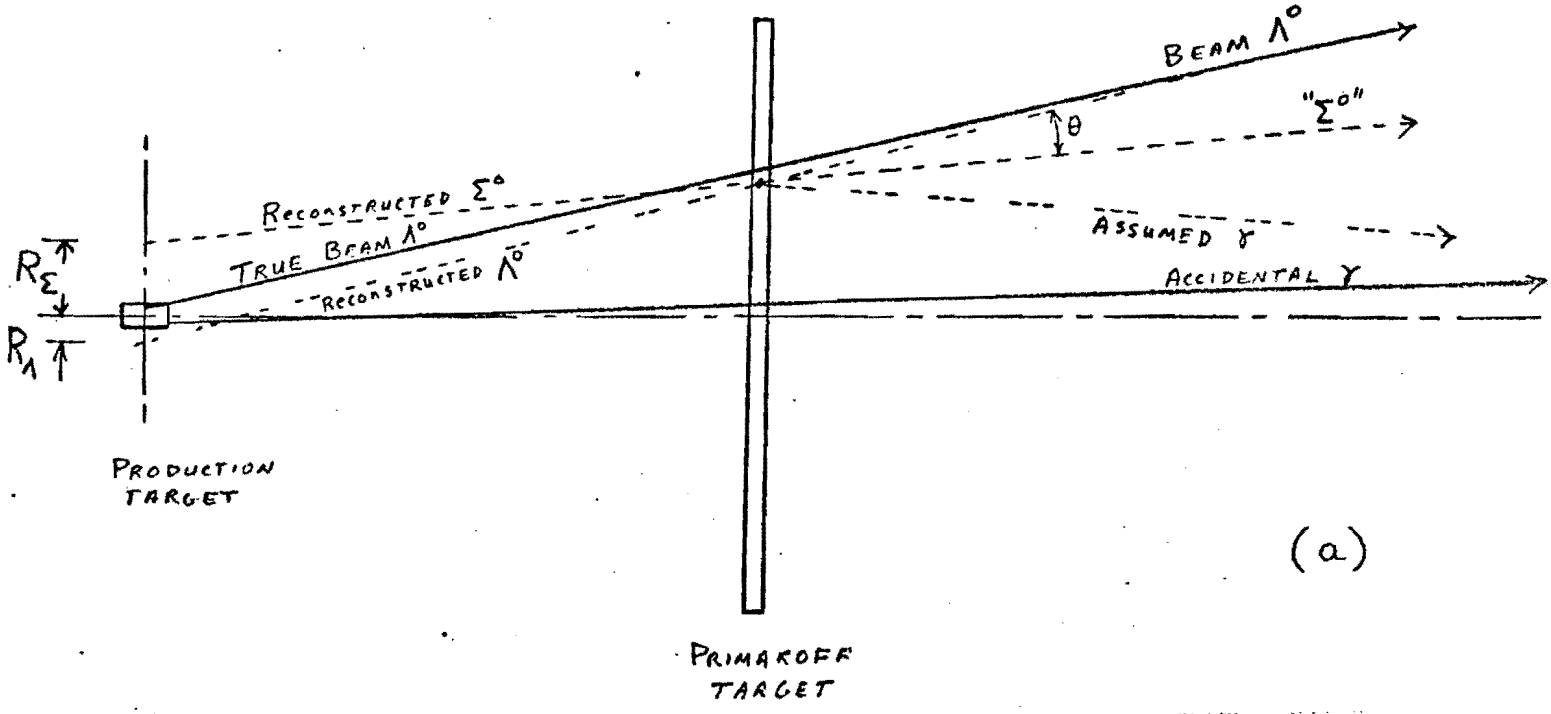
BEAM Λ°
"Σ°"
θ
RECONSTRUCTED Σ°
TRUE BEAM Λ°
RECONSTRUCTED Λ°
ASSUMED γ
ACCIDENTAL γ
R_Σ
R_Λ
PRODUCTION TARGET
PRIMAKOFF TARGET

(a)

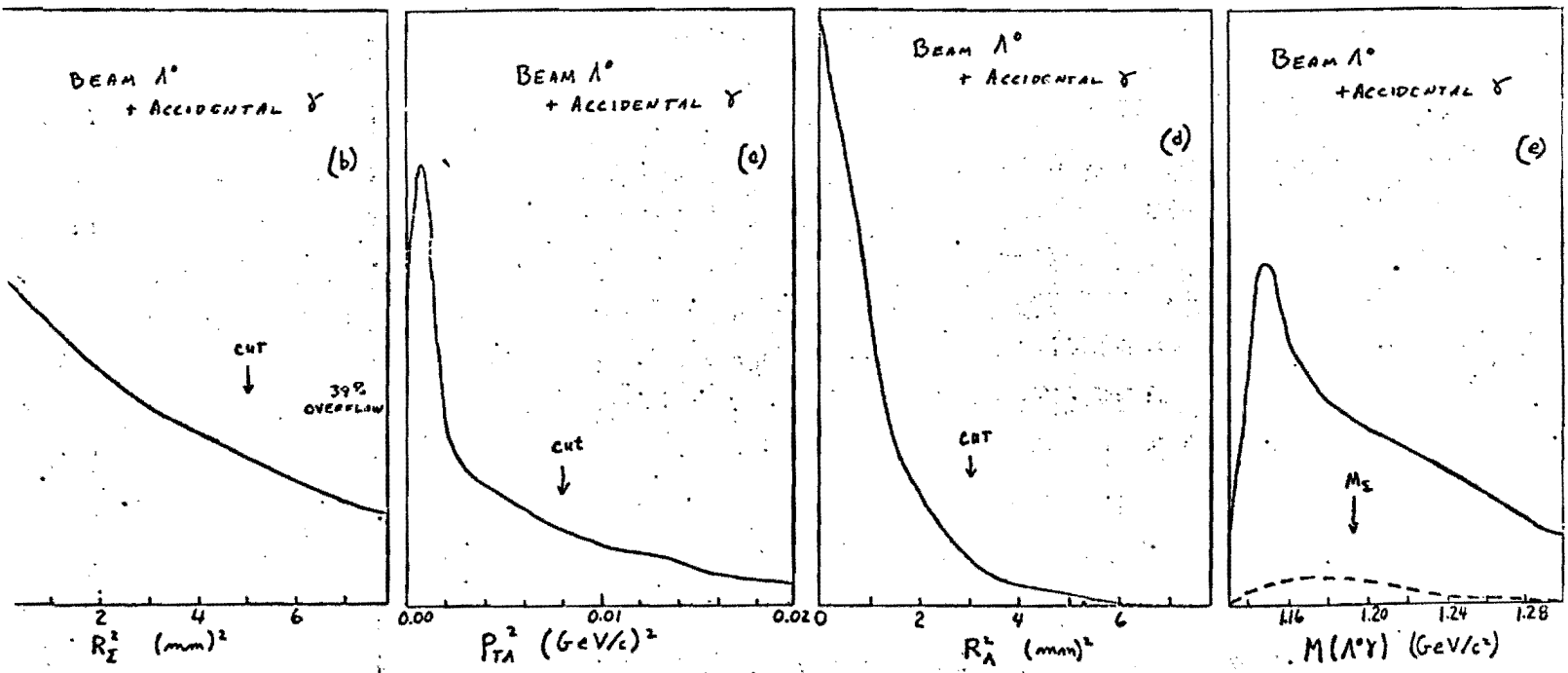
BEAM Λ°
+ ACCIDENTAL γ
(b)
CUT
39% OVERFLOW
2
4
6
R_Σ^2 (mm)²
BEAM Λ°
+ ACCIDENTAL γ
(c)
CUT
0.00
0.01
0.02
P_{TA}^2 (GeV/c)²
BEAM Λ°
+ ACCIDENTAL γ
(d)
CUT
0
2
4
6
R_Λ^2 (mm)²
BEAM Λ°
+ ACCIDENTAL γ
(e)
M_Σ
1.16
1.20
1.24
1.28
M(Λ°γ) (GeV/c²)

Fig. 5

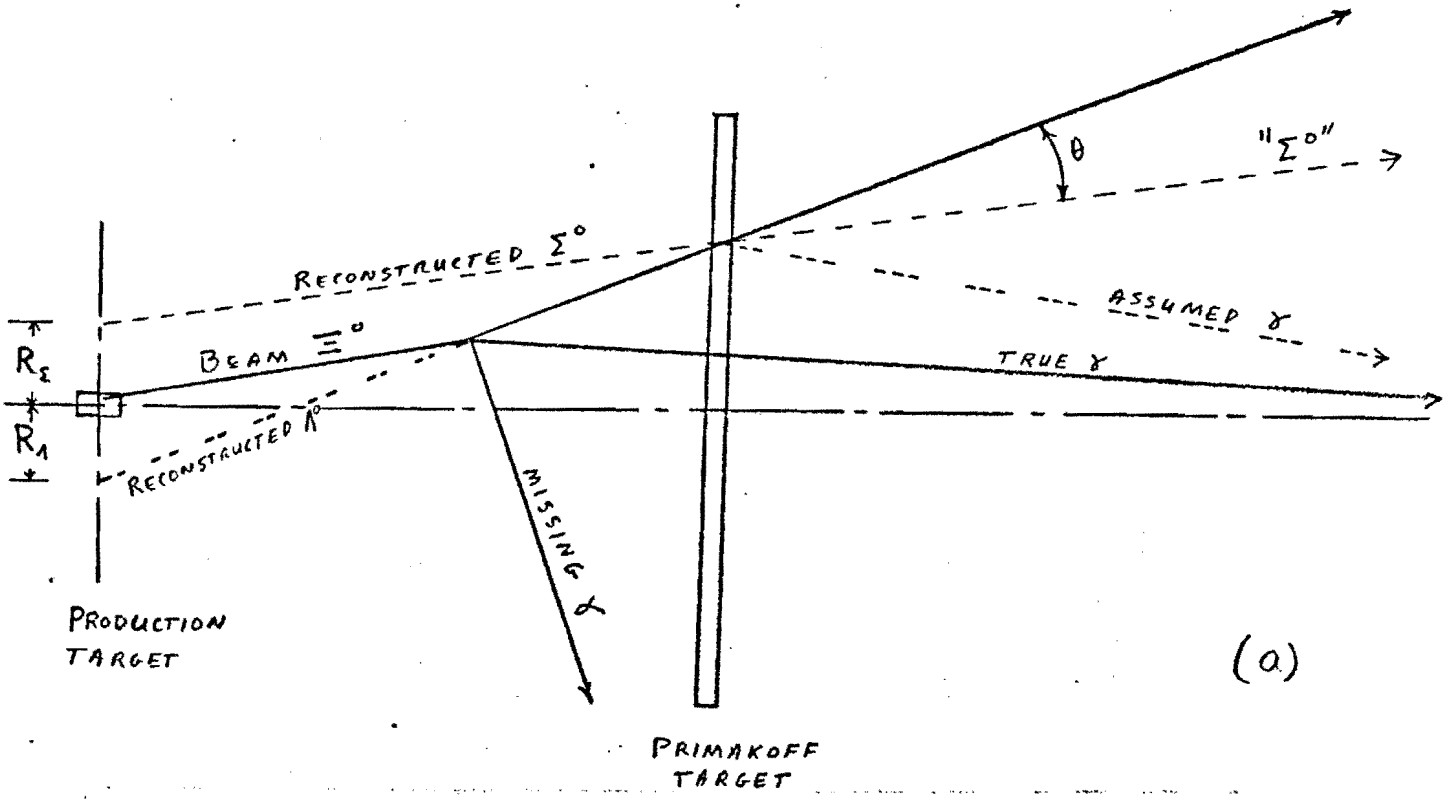
RECONSTRUCTED Σ°
BEAM Ξ°
RECONSTRUCTED Λ°
R_Σ
R_Λ
θ
"Σ°"
ASSUMED γ
TRUE γ
MISSING γ
PRODUCTION TARGET
PRIMAKOFF TARGET
(a)

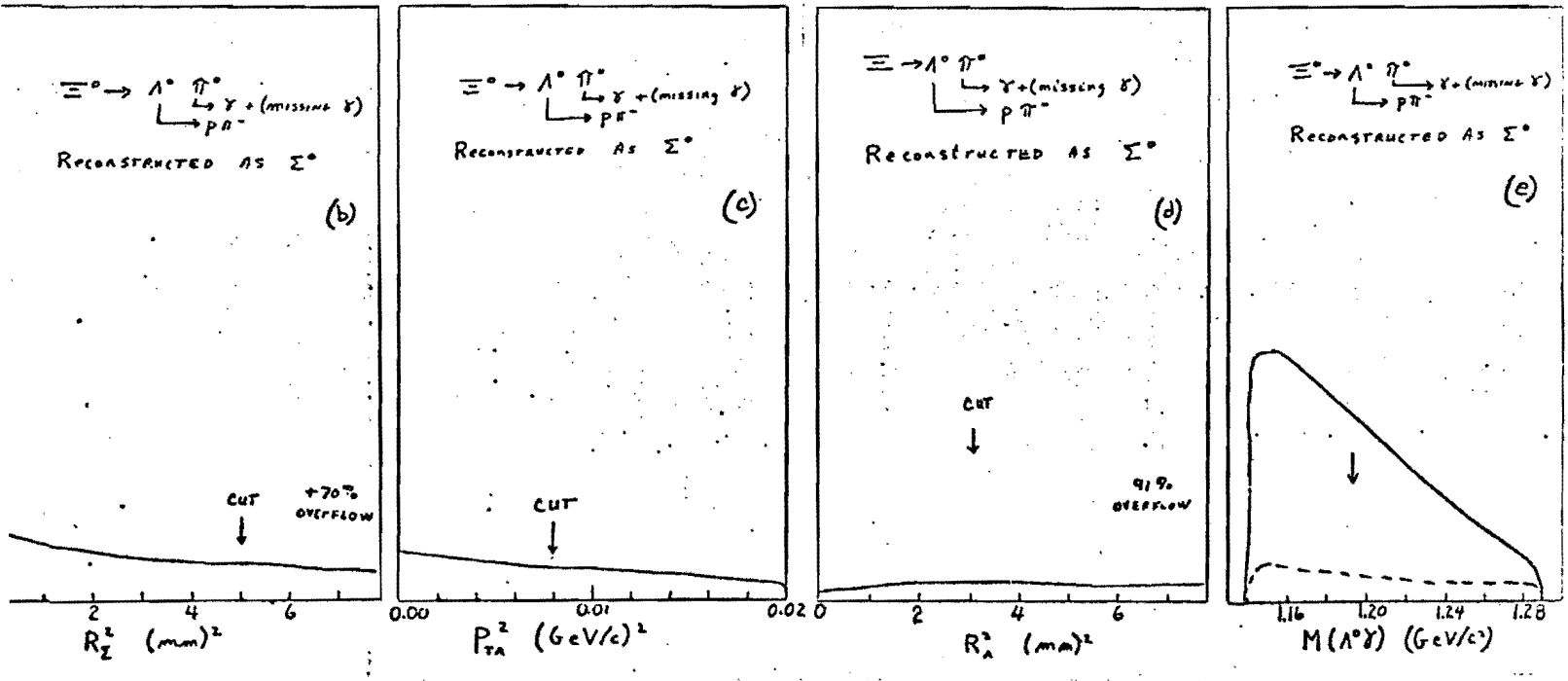
Ξ° → Λ° π°, γ + (missing γ), pπ⁻
RECONSTRUCTED AS Σ°
(b)
CUT
+70% OVERFLOW
R_Σ^2 (mm)²
(c)
P_{TA}^2 (GeV/c)²
(d)
91% OVERFLOW
R_Λ^2 (mm)²
(e)
M(Λ°γ) (GeV/c²)

Fig. 6